Enhanced mobility of confined polymers

KYUSOON SHIN[1]*, SERGEI OBUKHOV[2], JIUN-TAI CHEN[3], JUNE HUH[4], YOONTAE HWANG[1], SOONCHUN MOK[1], PRIYANKA DOBRIYAL[3], PAPPANNAN THIYAGARAJAN[5] AND THOMAS P. RUSSELL[3]*

[1]School of Chemical and Biological Engineering, Seoul National University, Seoul 151-744, South Korea
[2]Department of Physics, University of Florida, Gainesville, Florida 32611, USA
[3]Department of Polymer Science and Engineering, Silvio O. Conte National Center for Polymer Research, University of Massachusetts Amherst, Massachusetts 01003, USA
[4]School of Material Science and Engineering and Hyperstructured Organic Materials Research Center, Seoul National University, Seoul, 151-744, South Korea
[5]Intense Pulsed Neutron Source Division, Argonne National Laboratory, 9700 S. Cass Ave, Argonne, Illinois 60439-4814, USA
*e-mail: shin@snu.ac.kr; russell@mail.pse.umass.edu

Published online: 14 October 2007; doi:10.1038/nmat2031

Non-classical behaviour, brought about by a confinement that imposes spatial constraints on molecules, is opening avenues to novel applications. For example, carbon nanotubes, which show rapid and selective transport of small molecules across the nanotubes, have significant potential as biological or chemical separation materials for organic solvents or gaseous molecules[1–5]. With polymers, when the dimensions of a confining volume are much less than the radius of gyration, a quantitative understanding of perturbations to chain dynamics due to geometric constraints remains a challenge[6–10] and, with the development of nanofabrication processes, the dynamics of confined polymers have significant technological implications[11–17]. Here, we describe a weak molecular-weight-dependent mobility of polymers confined within nanoscopic cylindrical pores having diameters smaller than the dimension of the chains in the bulk. On the basis of the chain configuration along the pore axis, the measured mobility of polymers in the confined geometry is much higher than the mobility of the unconfined chain. With the emergence of nanofabrication processes based on polymer flow, the unexpected enhancement in flow and reduction in intermolecular entanglements are of significant importance in the design and execution of processing strategies.

Scaling arguments on the diffusion of single-chain molecules in the bulk predict that the reptation time of individual chains is proportional to the cube of the contour length[18]. Confinement, however, may influence the interpenetration of chains owing to the finite space available and the molecular-weight dependence of chain dynamics. Here, we address both issues in a study on the flow of polymers into nanoscopic cylindrical channels.

The capillary rise of a polymeric liquid in a nanoporous membrane has been studied recently. Anodized alumina membranes having cylindrical nanoscopic pores, with diameters comparable to or smaller than the radius of gyration of a polymer chain in the bulk, were used. Figure 1a shows a field-emission scanning electron micrograph of polystyrene nanorods ($M_w \sim 5.91 \times 10^5\,g\,mol^{-1}$) prepared using nanoporous alumina (pore diameter ~ 15 nm). As twice the radius of gyration, $2R_g$ ($\sim$45 nm), is approximately three times the pore diameter, the chain configuration must be perturbed, resulting in an entropic penalty due to chain deformation[10]. Despite this entropic penalty, the capillary force in the nanoscopic cylindrical pores is sufficiently strong to draw the polymer into the pore. The capillary rise of a polymer, polystyrene, in the pores (as shown in Fig. 1d) was measured by time-resolved small-angle X-ray scattering (SAXS) at $T \sim 190\,^{\circ}C$. The integrated intensity or the scattering invariant, Q, is proportional to $[\phi_U\rho_{AO}^2 + \phi_F(\rho_{AO} - \rho_{PS})^2]\phi_P\phi_{AO}$ where ϕ_P and ϕ_{AO} are the volume fractions of pores and alumina in the membrane, respectively, ϕ_U and ϕ_F are the volume fractions of unfilled and filled pores, respectively, and ρ_{AO} ($\sim$1.37 mole electrons cm^{-3}) and ρ_{PS} ($\sim$0.565 mole electrons cm^{-3}) are the electron densities of the aluminium oxide and polystyrene, respectively[19,20]. As $\phi_U = 1 - \phi_F$, then all of the parameters defining the invariant are known with the exception of the volume fraction of unfilled pores. As ϕ_U decreases, that is, as the pores fill, the integrated scattering decreases. Figure 1b shows the reduction in Q relative to Q_0, Q of the unfilled membrane at time $t = 0$, with time, that is, as the polystyrene rises in the pores. The total flux of polystyrene into the pores is given by:

$$J = \pi r^2 \frac{\Delta l}{\Delta t} = -K\frac{\Delta(Q/Q_0)}{\Delta t}, \qquad (1)$$

where r is the radius of the pore, l is the distance the polymer has flowed into the membrane and K ($\sim 3.24 \times 10^{-20}$ m^3) is $\pi r^2 L\rho_{AO}^2/(2\rho_{AO} - \rho_{PS})\rho_{PS}$. L ($\sim$120 μm) is the length of the nanopore. So, from equation (1), the flux of the polymer into the pores can be determined and compared with that expected from the bulk viscosity of the polymer[21,22].

It is striking that the flux is only weakly molecular-weight dependent as shown in Fig. 1c. As the flux is inversely proportional to $\sim N^{1.5\pm0.1}$, and as the flux is inversely related to the viscosity, η, then $\eta \sim N^{1.5\pm0.1}$. In the bulk, the reptative motion of polymer chains predicts $\eta \sim N^{3.4}$ above the entanglement molecular weight, M_e, of the polymer[23–25]. For polystyrene, $M_e \sim 2 \times 10^4\,g\,mol^{-1}$, the molecular-weight dependence observed here for flow into the nanopores is much less than that reported for the bulk. Consequently, confinement has markedly decreased η, enhancing the flow of polystyrene when $N > N_e$. As an example, η for polystyrene ($M_w \sim 1.03 \times 10^6\,g\,mol^{-1}$) in the bulk is 4.4×10^6 Pa s (ref. 21), whereas in the nanopores ($d \sim 15$ nm) η, evaluated using the Washburn equation[23], is 3.4×10^3 Pa s. The slope of $1 - Q/Q_0$ versus the square root of time in Fig. 1b was $0.056\,h^{-1/2}$ for the polystyrene ($M_w \sim 1.03 \times 10^6\,g\,mol^{-1}$), and the surface tension of

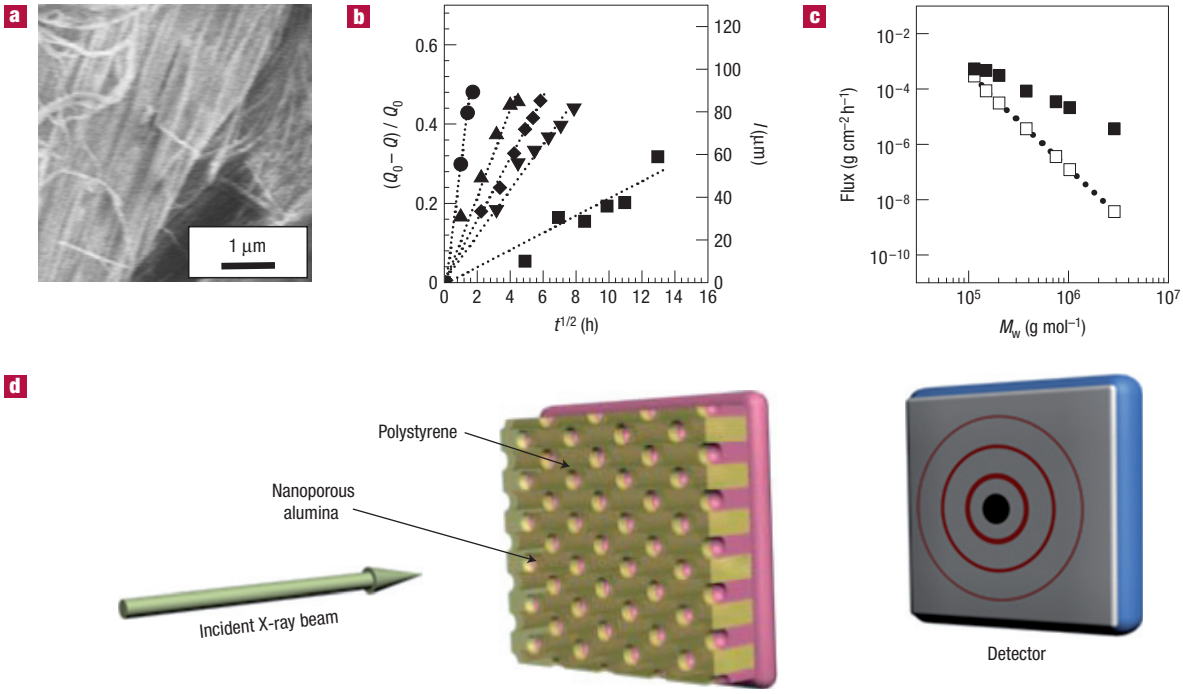

Figure 1 Measurement of capillary rise of polymeric liquid. a, Scanning electron micrograph of polystyrene nanorods ($M_w \sim 591$ kg mol^{-1}) prepared from nanoporous alumina. **b**, Scattering invariant and the height of the polystyrene in the nanoporous alumina as a function of the square root of the heating time. From the steepest increase, M_w is 114 (filled circles), 379 (filled triangles), 750 (filled diamonds), 1,032 (filled down-triangles), 2,880 (filled squares) kg mol^{-1}, respectively. As the polymeric melt fills the pore, the electron density difference between the alumina matrix and the cylindrical pore becomes lower. **c**, The flux of polystyrene melt of different molecular weights (filled squares) through the nanoporous alumina ($d \sim 15$ nm, $L \sim 120$ μm) when $l \sim L/2$, and the flux calculated with the bulk property (open squares and line) from ref. 22. **d**, Schematic diagram of the SAXS experiment to measure the capillary rise in the nanoscopic cylindrical pores.

polystyrene (ref. 26) and the contact angle between polystyrene and alumina, used for the evaluation of η, was ~29 mJ m^{-2} and ~23°, respectively. Typically, this polystyrene penetrates ~100 μm into the pores over the course of a day, which is slow enough not to stretch the chain molecules during flow in the nanopores.

The segmental mobility of chain molecules in the cylindrical nanopores was also investigated. Differential scanning calorimetry studies of polystyrene in the nanopores are shown in Fig. 2. Several different molecular weights of polystyrene in the nanoporous alumina ($d \sim 15$ nm) were examined. As shown in the figure, the glass-transition region of polystyrene in the nanoporous alumina was broader than that of bulk, and the glass-transition behaviour of polystyrene in the nanoporous alumina, similar to results on supported ultrathin films[27–30], showed little dependence on the molecular weight. The onset point or end point of the glass transition varied by only 10 K and was essentially the same as that measured for polystyrene on supported thin films. This is understandable, as the polymer in the pores can be considered as an extension of the case of thin films on a support[31–33]. As flow measurements were done well above the end point of the transition of polystyrene in the nanopores and the glass-transition behaviour was not relevant to the molecular weight, the observed reduction in η cannot be attributed to the glass-transition temperature, T_g.

The conformation of polystyrene in the nanopores was measured by small-angle neutron scattering (SANS) using a 0.1-mm-thick alumina membrane filled with a mixture of 61% deuterated polystyrene and 39% hydrogenous polystyrene. The nanoporous channels were partially filled, to avoid an overflow of the polymer melt onto the surface. The remaining unfilled portions of the nanopores were filled with a contrast-matching fluid (d-ethanol/h-ethanol) to remove excess scattering from the membrane. The fraction of deuterated polystyrene and hydrogenous polystyrene was chosen so that the neutron scattering-length density of the deuterated polystyrene/hydrogenous polystyrene mixture matched that of the membrane so as to minimize any scattering from the membrane and improve the signal-to-noise ratio of the single-chain scattering. The polymer-filled membrane was placed in the neutron beam and tilted to an incidence angle of 30° (as shown in Fig. 3a). A typical SANS profile of a deuterated polystyrene/hydrogenous polystyrene (61 wt% deuterated polystyrene, M_w of deuterated polystyrene ~ 528 kg mol^{-1} and M_w of hydrogenous polystyrene ~ 591 kg mol^{-1}) mixture in an anodic aluminium oxide membrane with 30-nm-diameter pores is shown in Fig. 3b. Any residual scattering arising from the membrane occurs on the horizon ($q_y = 0$) and, as would be expected, a reflection is seen at $q \sim 0.01$ Å^{-1} corresponding to the centre-to-centre distance between the pores. Even although a contrast-matching condition was used, any slight mismatch will result in a substantial amount of scattering relative to any other contributions to the scattering. The SANS along q_z, that is, in the direction of the axes of the pores, has two origins. The first is the form factor of the pores and, as the length of the pores is large, this scattering occurs at angles well beyond the resolution of the instrument and can be ignored. The second, which is much weaker, arises from the single-chain scattering of the deuterated polystyrene/hydrogenous polystyrene mixture confined in the pores. Figure 4a shows the scattering pattern along q_z (filled squares and circles) taken from the two-dimensional pattern in Fig. 3b and the calculated single-chain scattering (solid line, Debye function).

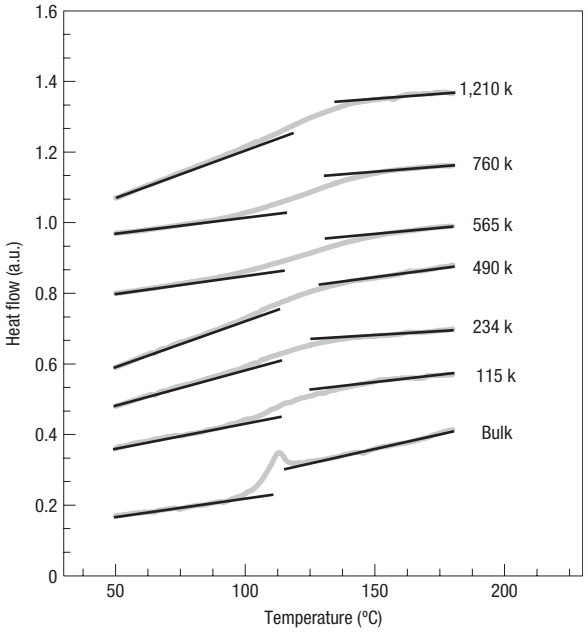

Figure 2 Differential scanning calorimetry of polystyrene in the cylindrical nanoporous alumina. The pore diameter of the alumina was 15 nm, and the heating rate was 30 K min^{-1}. The bottom thermogram is for bulk polystyrene ($M_w \sim 1{,}210$ k) and the other thermograms are those of polystyrene in nanopores.

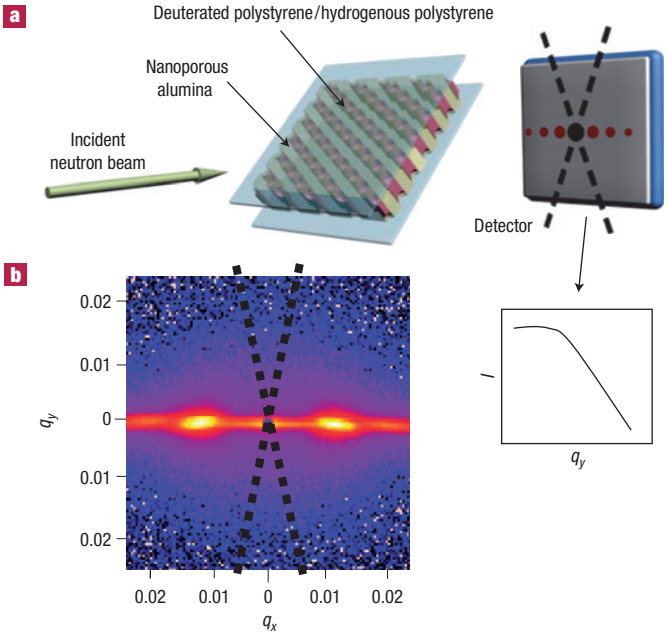

Figure 3 Measurement of overall conformation along nanopore axes via SANS experiment. a, Schematic diagram of SANS set-up, showing the collimated incident beam, oriented sample, an area detector and the averaged scattered intensity over a range of span from the vertical axis. The uniformly oriented polymer-containing nanopores are tilted to an incidence angle of 30° relative to the normal incidence of the beam. **b**, Typical two-dimensional scattering pattern of deuterated polystyrene/hydrogenous polystyrene (61 wt% deuterated polystyrene, M_w of deuterated polystyrene ~ 528 kg mol^{-1} and M_w of hydrogenous polystyrene ~ 591 kg mol^{-1}) in a nanoporous alumina template (pore diameter ~ 30 nm). The strong bright spots, the lattice scattering due to the regular spacing between the cylindrical pores, appear only horizontally as the aligned pores are tilted 30° relative to the normal incidence of the beam. The scattering intensity was averaged with a span of $\pm 10°$ from the vertical axis to analyse the overall chain dimension along pore axes. The span is shown as black dotted lines.

The scattering from bulk polystyrene is also shown for comparison. For $q > 0.002$ Å^{-1}, these data are well described by the calculated profile of an unperturbed chain. Consequently, along the pore axis, the chain is unperturbed. The radius of gyration of the polymer in the nanopores was found to be identical to that in the bulk over a wide range of molecular weights and pore diameters, as shown in Fig. 4b. This is consistent with theoretical arguments[18,34,35]. As the chain is unperturbed along the pore axis and the pore diameter is less than $2R_g$, then, assuming incompressibility of the polymer melt, the number of chains per unit volume must be smaller than that in the bulk. The polymer chain is confined inside the volume $V_{pore} = \pi b N^{1/2} r^2$, where b is the Kuhn segment length. In a bulk, the same chain would be confined inside the volume $V_{bulk} = (\pi/6)[bN^{1/2}]^3$. When the density of a polymer melt is the same as the density in the bulk, we have to conclude that the number of chains sharing the same volume V_{pore} is smaller than the number of chains sharing the volume V_{bulk}. However, the pore size is still large, compared with the chain segments ($b \ll 2r < 2R_g$), and the polymers in the pores are not fully disentangled in the molecular-weight regime that we have used. Therefore, it is reasonable to use the single-chain scattering with the assumption that the complete demixing of protonated and deuterated chains does not occur.

These results suggest that, as the entangled polymer enters and flows into the pores, the number of chains per unit volume is decreased and, consequently, the interpenetration of the polymer chains decreases. However, after flow into the pores the chains are not stretched in the direction of flow but, owing to confinement, are compressed in a direction orthogonal to the flow. The diffusivity of a single unperturbed chain in a polymer melt is known to be proportional to $N^{-2.4\pm0.1}$ and can be written as ($N > N_e$ limit)[23–25]: $\mu \approx N_e^{1.4}/\eta_0 b N^{2.4}$, where η_0 and N_e are the segmental viscosity and entanglement length, respectively. The average force applied to each polymer chain is produced by a pressure gradient p' is $F = p' b^3 N$.

Calculating the average drift velocity in a nanotube $v = \mu F$, and multiplying it by the cross-sectional area of the nanotube, the total flux, J, will be $\sim F\mu\kappa N/R_{g,ll}$, where κ is the number of polymers sharing the same volume and κN is the total number of monomers inside the tube length $R_{g,ll}$. Using $\kappa = r^2 b/N^{1/2}$, we obtain:

$$J = F\mu r^2 = \frac{p' b^2 r^2}{\eta_0}\left(\frac{N_e}{N}\right)^{1.4} \quad (2)$$

Equation (2) shows that the flux is proportional to $\sim N^{-1.4}$. As the apparent viscosity of the polymer is inversely proportional to the flux, the apparent viscosity should be proportional to $\sim N^{1.4}$. This simple scaling argument agrees well with our experimental observations.

Whereas no apparent mobility change has been observed for small molecules in interconnected nanopores[36], the large chain molecules were found to have an enhanced mobility in this confining geometry. In a melt of a bulk semicrystalline polymer, a change in the flow behaviour due to a decrease of the degree of chain interpenetration was reported. It was recently found that the entanglement density could be controlled by slow melting and the long-lived less-entangled melt had a lower melt viscosity and enhanced drawability[37]. In addition to the enhanced flow, confinement effects on the chain conformation can perturb the

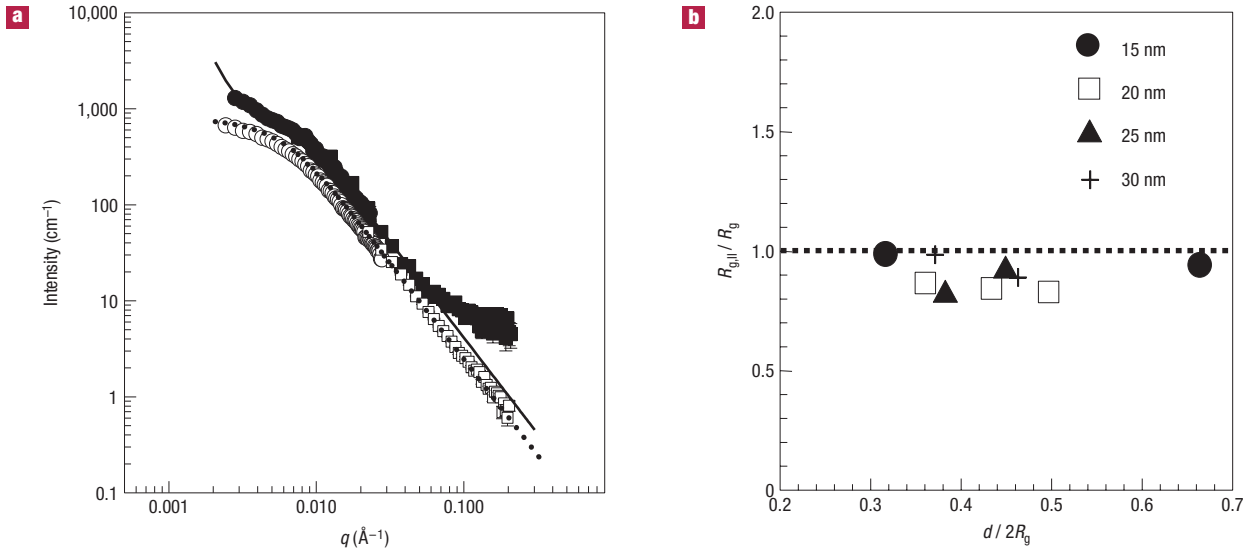

Figure 4 Scattered intensity of polystyrene in bulk and in nanopores from two-dimensional SANS pattern after calibration and the chain dimensions of different molecular-weight polystyrene along the pore axes in different pore diameters. a, The averaged SANS pattern (with a $\pm 10^{\circ}$ span with a centre of the vertical axis) from Fig. 3b of deuterated polystyrene/hydrogenous polystyrene (61 wt% deuterated polystyrene, M_w of deuterated polystyrene $\sim$ 528 kg mol^{-1} and M_w of hydrogenous polystyrene $\sim$ 591 kg mol^{-1}) in the nanopore (pore diameter $\sim$ 30 nm). The open symbols are the experimental data of bulk deuterated polystyrene/hydrogenous polystyrene, and the filled symbols are the scattering of deuterated polystyrene/hydrogenous polystyrene in the nanoporous membrane. The dotted and solid lines are the RPA function fitted for the mixture in bulk and in the nanoporous membrane, respectively. The raw data were calibrated for empty cell, detector efficiency and relative to standard materials, and then they were plotted on an absolute intensity scale. Circular and square symbols are in different q ranges, and they were obtained at NIST and IPNS, respectively. **b**, The chain dimension along the nanopore axis relative to the radius of gyration in bulk as a function of the ratio of pore diameter to twice the radius of gyration.

interfacial properties and, ultimately, the long-term stability of the nanostructured materials.

METHODS

Nanoporous alumina was prepared by an electrochemical two-step anodization method in dilute sulphuric acid (0.3 M) with an applied voltage of 25 V. A highly pure aluminium plate (Aldrich, 99.998%, thickness $\sim$ 1 mm) was electropolished and anodized. After chemical etching with phosphochromic acid, the second anodization was carried out for 24 h. The aluminium supporting layer was dissolved in cuprous chloride solution. The pore was then opened by floating the membrane on dilute phosphoric acid (0.3 M) followed by rinsing in an ethanol/water mixture (20/80). The home-made membrane had hexagonally packed straight pores that ran all the way through. The centre-to-centre distances of the pores were 65 nm, as determined by scanning electron microscopy analysis.

The capillary rise of the polymeric liquid into the pores was investigated by SAXS. The polymeric film was solution-cast onto a thin cover glass. After drying the film in ambient environment for several days, it was dried under vacuum for 3 days at 170 °C. Then, the dried film (thickness $\sim$ 100 μm) was preheated on a hot plate for several minutes, and the nanoporous alumina was placed on top of it. To ensure good contact between the membrane and the molten film, the membrane was gently tapped several times. After checking for good contact, the sample was moved to a vacuum oven that was preheated to 190 °C. The oven was evacuated and the sample was kept under vacuum. After some time, the sample was taken out of the vacuum oven, and quenched by placing the sample on a large Al plate. Then, the scattered intensity from the hexagonally packed pore was measured by SAXS. The scattering experiments were conducted at the 4C2 beamline at the Pohang Light Source ($\lambda = 1.38$ Å) or with a conventional instrument (Cu Kα source, $\lambda = 1.54$ Å, Rigaku).

For T_g measurement, polystyrene was selectively located in the nanopores[38]. A polystyrene film was prepared by solution casting. The polystyrene film was thoroughly dried, and then placed on a thick film of poly(2-vinylpyridine). Nanoporous alumina was placed on the bilayer film, and then the sample was heated to 190 °C under vacuum. The polystyrene melt was drawn into the nanopores via capillary force. After heating, the bottom layer poly(2-vinylpyridine) film was removed by immersing the sample in ethanol for several days. The glass-transition behaviour was examined at a heating rate of 30 K min^{-1} from room temperature after the ageing at 60 °C for 18 h.

The overall conformation in the nanopore was measured by SANS. Hydrogenous polystyrene (61 wt%) was mixed with deuterated polystyrene (39 wt%) in solution and a thin film was solvent cast. As in the sampling for the T_g measurement, using the bilayer method, we selectively locate the hydrogenous polystyrene/deuterated polystyrene mixture in the nanopore. The SANS measurements were carried out at the NG3 beamline in the NIST Center for Neutron Research at the National Institutes of Standards and Technology (NIST) in Gaithersburg, or the small-angle neutron diffractometer (SAND) at the Intense Pulsed Neutron Source (IPNS) at Argonne National Lab. The set-up in NIST was as follows: a wavelength (λ) of 4.31 Å and $\Delta\lambda/\lambda = 0.15$ at a sample-to-detector distance of 15 m. Contrast-matching experiments and scattering experiments for the high q range were done at the time-of-flight SAND beamline in IPNS at the Argonne National Laboratory. The wavelength at the SAND ranged from 1.1 to 14 Å, and the source frequency was 30 Hz. The sample-to-detector distance was 1.5 m. The hydrogenous polystyrene/deuterated polystyrene-containing nanoporous alumina was placed between two quartz plates, and it was immersed in a d-ethanol/h-ethanol mixture. Between the quartz plates, there was a rubbery spacer that prevented leakage of the ethanol mixture. The polystyrene-containing alumina was tilted 30° relative to the incident neutron beam. The scattering information on the chain conformation was taken from the vertical wedge-shaped cross-section of the scattered pattern (azimuthal angle: $\pm 10^{\circ}$). The background and dark current were subtracted from the measured intensity that was normalized to the incident beam intensity. Bulk samples with molecular weights corresponding to those in the nanopores were also examined.

Received 10 April 2007; accepted 13 September 2007; published 14 October 2007.

References

1. Holt, J .K. *et al.* Fast mass transport through sub-2-nanometer carbon nanotubes. *Science* **312**, 1034–1037 (2006).
2. Majumder, M., Chopra, N., Andrews, R. & Hinds, B. J. Nanoscale hydrodynamics: Enhanced flow in carbon nanotubes. *Nature* **438**, 44 (2005).

3. Hummer, G., Rasaiah, J. C. & Noworyta, J. P. Water conduction through the hydrophobic channel of a carbon nanotube. *Nature* **414**, 188–190 (2001).
4. Kaira, A., Garde, S. & Hummer, G. Osmotic water transport through carbon nanotube membranes. *Proc. Natl Acad. Sci. USA* **100**, 10175–10180 (2003).
5. Skoulidas, A. I., Ackerman, D. M., Johnson, J. K. & Sholl, D. S. Rapid transport of gases in carbon nanotubes. *Phys. Rev. Lett.* **89**, 185901 (2002).
6. Frank, B., Gast, A. P., Russell, T. P., Brown, H. R. & Hawker, C. J. Polymer mobility in thin films. *Macromolecules* **29**, 6531–6534 (1996).
7. Ellison, C. J. & Torkelson, J. M. The distribution of glass-transition temperatures in nanoscopically confined glass formers. *Nature Mater.* **2**, 695–700 (2005).
8. O'Connell, P. A. & McKenna, G. B. Rheological measurements of the thermoviscoelastic response of ultrathin polymer films. *Science* **307**, 1760–1763 (2005).
9. Zheng, X. *et al.* Reptation dynamics of a polymer melt near an attractive solid interface. *Phys. Rev. Lett.* **74**, 407–410 (1995).
10. Jones, R. L., Kumar, S. K., Ho, D. L., Briber, R. M. & Russell, T. P. Chain conformation in ultrathin polymer films. *Nature* **400**, 146–149 (1999).
11. Brown, H. R. Chain pullout and mobility effects in friction and lubrication. *Science* **263**, 1411–1413 (1994).
12. Granick, S. *et al.* Macromolecules at surfaces: Research challenges and opportunities from tribology to biology. *J. Polym. Sci. B* **41**, 2755–2793 (2003).
13. Suh, K. Y. & Lee, H. H. Capillary force lithography. *Adv. Mater.* **13**, 1386–1389 (2001).
14. Creton, C., Brown, H. R. & Shull, K. R. Molecular weight effects in chain pullout. *Macromolecules* **27**, 3174–3183 (1994).
15. Smith, G. D., Yoon, D. Y. & Jaffe, R. L. Long-time molecular motions and local chain dynamics in n-$C_{44}H_{90}$ melts by molecular dynamics simulations. *Macromolecules* **28**, 5897–5905 (1995).
16. Stafford, C. M. *et al.* A buckling-based metrology for measuring the elastic moduli of polymeric thin films. *Nature Mater.* **3**, 545–550 (2004).
17. Shin, K. *et al.* Curving and frustrating flatland. *Science* **306**, 76 (2004).
18. de Gennes, P. G. *Scaling Concepts in Polymer Physics* (Cornell Univ. Press, Ithaca, 1979).
19. Roe, R. *Methods of X-Ray and Neutron Scattering in Polymer Science* (Oxford Univ. Press, New York, 2000).
20. Balta-Calleja, F. J. & Vonk, C. G. *X-Ray Scattering of Synthetic Polymers* (Elsevier, Amsterdam, 1989).
21. Zosel, A. Der Einfluß von Molekulargewicht und Molekulargewichtsverteilung auf die viskoelastischen Eigenschaften von Polystyrolschmelzen. *Rheol. Acta* **10**, 215–224 (1971).
22. Washburn, E. W. The dynamics of capillary flow. *Phys. Rev.* **17**, 273–283 (1921).
23. Lodge, T. P. Reconciliation of the molecular weight dependence of diffusion and viscosity in entangled polymers. *Phys. Rev. Lett.* **83**, 3218–3221 (1999).
24. Doi, M. & Edwards, S. F. *The Theory of Polymer Dynamics* (Oxford Univ. Press, New York, 1986).
25. Tao, H., Lodge, T. P. & von Meerwall, E. D. Diffusivity and viscosity of concentrated hydrogenated polybutadiene solutions. *Macromolecules* **33**, 1747–1758 (2000).
26. Brandrup, J. & Immergut, E. H. *Polymer Handbook* 3rd edn (Wiley Interscience, New York, 1989).
27. Keddie, J. L., Jones, R. A. L. & Cory, R. A. Size-dependent depression of the glass transition temperature in polymer films. *Europhys. Lett.* **27**, 59–64 (1994).
28. Keddie, J. L., Jones, R. A. L. & Cory, R. A. Interface and surface effects on the glass transition temperature in thin polymer films. *Faraday Discuss.* **98**, 219–230 (1994).
29. DeMaggio, G. B. *et al.* Interface and surface effects on the glass transition in thin polystyrene films. *Phys. Rev. Lett.* **78**, 1524–1527 (1991).
30. Efremov, M. Y., Olson, E. A., Zhang, M., Zhang, Z. & Allen, L. H. Glass transition in ultrathin polymer films: Calorimetric study. *Phys. Rev. Lett.* **91**, 085703 (2003).
31. Park, J. & McKenna, G. B. Size and confinement effects on the glass transition behavior of polystyrene/o-terphenyl polymer solutions. *Phys. Rev. B* **61**, 6667–6676 (2000).
32. Pissis, P., Kyritsis, A., Barut, G., Pelster, R. & Nimtz, G. Glass transition in 2- and 3-dimensionally confined liquids. *J. Non-Cryst. Solids* **235–237**, 444–449 (1998).
33. Bansal, A. *et al.* Quantitative equivalence between polymer nanocomposites and thin polymer films. *Nature Mater.* **4**, 693–698 (2005).
34. Kumar, S. K., Vacatello, M. & Yoon, D. Y. Off-lattice Monte Carlo simulations of polymer melts confined between two plates. *J. Chem. Phys.* **89**, 5206–5216 (1988).
35. Rubinstein, M. & Colby, R. H. *Polymer Physics* (Oxford Univ. Press, New York, 2003).
36. Huber, P., Grüner, S., Schäfer, C., Knorr, K. & Kityk, A. V. Rheology of liquids in nanopores: A study on the capillary rise of water, *n*-Hexadecane and *n*-Tetracosane in mesoporous silica. *Eur. Phys. J. Special Topics* **141**, 101–105 (2007).
37. Rastogi, S. *et al.* Heterogeneity in polymer melts from melting of polymer crystals. *Nature Mater.* **4**, 635–641 (2005).
38. Woo, E., Huh, J., Jeong, Y. G. & Shin, K. From homogeneous to heterogeneous nucleation of chain molecules under nanoscopic cylindrical confinement. *Phys. Rev. Lett.* **98**, 136103 (2007).

Acknowledgements

This work was supported by the Korea Research Foundation (MOEHRD, Basic Research Promotion Fund for new faculties, KRF-2006-331-D00160) and the Korea Science and Engineering Foundation (Basic Research Program, R01-2006-000-10749-0). K.S. and S.M. are indebted to the experimental support staff of the 4C2 beamline at the Pohang Light Source. T.P.R., P.D. and J.-T.C. were supported by the Department of Energy Basic Energy Sciences (DEFG0296ER45612) and the National Science Foundation-supported Material Research Science and Engineering Center at the University of Massachusetts, Amherst (DMR-0213695). S.O. acknowledges the support of Petroleum Research Grant PRF# 43923 -AC 7 and the hospitality of ICS Strasbourg. Use of IPNS was supported by the Department of Energy Basic Energy Sciences (DE-AC02-06CH11357).
Correspondence and requests for materials should be addressed to K.S. or T.P.R.

Author contributions

All authors participated in discussions of the research and wrote the manuscript. K.S. and S.M. measured capillary rise. S.O. and J.H. developed theory. Y.H. observed glass transition. K.S., J.-T.C., S.M., P.D., P.T. and T.P.R. carried out the overall conformation measurements.